AD-A047 822 NAVAL RESEARCH LAB WASHINGTON D C F/G 20/9
GENERATION OF A REVERSED-FIELD PLASMA, CONFINEMENT CONFIGURATIO--ETC(U)
NOV 77 J D SETHIAN, D A HAMMER, K A GERBER

UNCLASSIFIED NRL-MR-3648 SBIE-AD-E000 069 NL

1 OF 1
ADA047822

END
DATE FILMED
1-78
DDC

NRL Memorandum Report 3648

Generation of a Reversed-Field Plasma Confinement Configuration with a Rotating Relativistic Electron Beam

J. D. SETHIAN, D. A. HAMMER, K. A. GERBER, D. N. SPECTOR and A. E. ROBSON

Experimental Plasma Physics Branch
Plasma Physics Division

and

G. C. GOLDENBAUM

Department of Physics and Astronomy
University of Maryland, College Park, MD 20742

November 1977

NAVAL RESEARCH LABORATORY
Washington, D.C.

SECURITY CLASSIFICATION OF THIS PAGE (When Data Entered)

REPORT DOCUMENTATION PAGE

READ INSTRUCTIONS BEFORE COMPLETING FORM

1. REPORT NUMBER: NRL Memorandum Report 3648
2. GOVT ACCESSION NO.
3. RECIPIENT'S CATALOG NUMBER

4. TITLE (and Subtitle): GENERATION OF A REVERSED-FIELD PLASMA CONFINEMENT CONFIGURATION WITH A ROTATING RELATIVISTIC ELECTRON BEAM,
5. TYPE OF REPORT & PERIOD COVERED: Interim report on a continuing NRL Problem.
6. PERFORMING ORG. REPORT NUMBER

7. AUTHOR(s): J.D. Sethian, D.A. Hammer*, K.A. Gerber, D.N. Spector, A.E. Robson, and G.C. Goldenbaum
8. CONTRACT OR GRANT NUMBER(s)

9. PERFORMING ORGANIZATION NAME AND ADDRESS: Naval Research Laboratory, Washington, D.C. 20375
10. PROGRAM ELEMENT, PROJECT, TASK AREA & WORK UNIT NUMBERS: NRL Problem H02-28B

11. CONTROLLING OFFICE NAME AND ADDRESS
12. REPORT DATE: November 1977
13. NUMBER OF PAGES: 41

14. MONITORING AGENCY NAME & ADDRESS (if different from Controlling Office): 12 42p. 14 NRL-MR-3648
15. SECURITY CLASS. (of this report): UNCLASSIFIED
15a. DECLASSIFICATION/DOWNGRADING SCHEDULE

16. DISTRIBUTION STATEMENT (of this Report): Approved for public release; distribution unlimited. 18 SBIE 19 AD-E000 069

17. DISTRIBUTION STATEMENT (of the abstract entered in Block 20, if different from Report)

18. SUPPLEMENTARY NOTES: *Present address — Laboratory of Plasma Studies, Cornell University, Ithaca, New York.

19. KEY WORDS (Continue on reverse side if necessary and identify by block number): Reversed fields; Rotating relativistic electron beam; Belt-pinch

20. ABSTRACT (Continue on reverse side if necessary and identify by block number)

A reversed-field plasma confinement geometry has been produced by plasma currents induced by a rotating relativistic electron beam injected into 85 mTorr neutral hydrogen. The resulting belt-pinch-like configuration has a rectangular cross-section, with length-to-width ratio of 20, and a midplane $\beta = .5$. An equilibrium model, fitted to measurements of the excluded flux and induced axial (ΔB_z) and azimuthal (B_θ) magnetic fields, is in agreement with the annular plasma profile observed with radial Thomson scattering scans, CO_2 interferometry and end-on streak
(Continues)

DD FORM 1 JAN 73 1473 EDITION OF 1 NOV 65 IS OBSOLETE S/N 0102-014-6601

SECURITY CLASSIFICATION OF THIS PAGE (When Data Entered)

251 950

20. ABSTRACT (Continued)

photographs. After beam passage, ΔB_θ remains constant for 5 μsec until B_θ becomes small, at which time the plasma collapses radially. The observed decay times of 4 μsec, and concurrent increase in T_e (from 5-to-10eV) are consistent with classical dissipation of the induced currents.

CONTENTS

GENERATION OF A REVERSED-FIELD PLASMA CONFINEMENT CONFIGURATION WITH A ROTATING RELATIVISTIC ELECTRON BEAM

I. Introduction

It has recently been proposed to produce a reversed-field plasma confinement configuration with a rotating relativistic electron beam.[1] This paper describes initial studies of such a configuration, which is similar to an elongated cross-section Tokamak or a Belt Pinch[2] (see Fig. 1), and is formed by beam-induced azimuthal and axial plasma currents of sufficient magnitude to reverse the applied axial (poloidal) field on axis, and produce a comparable azimuthal (toroidal) field, respectively. As the induced currents persist long after beam passage, a plasma confined by such a configuration, once set up, can be heated further by magnetic compression (for example, by imploding metallic liners[3]), or by injection of high energy neutral beams (as in 2 × IIB[4]).

The formation of this reversed-field configuration is shown schematically in Figs. 2a-2d. (For simplicity, only the aximuthal currents and axial magnetic fields are shown.) A rotating relativistic electron beam, produced by passing an annular beam through a magnetic cusp, is injected along an applied magnetic field, B_o, into a conducting chamber containing neutral hydrogen gas. The large dB/dt at the

Note: Manuscript submitted November 9, 1977.

beam front induces an electric field that breaks down the gas and induces a return current, i.e. plasma currents in a direction counter to the beam current. The neutral gas pressure is chosen such that breakdown is fast enough to allow a sufficiently dense plasma for beam propagation, but slow enough to keep the rise in conductivity, and consequently the return current, small. In other words, the beam is charge-, but not current-, neutralized. Thus, large net current densities will be generated across ($j_{\theta\text{-net}}$) and along ($j_{z\text{-net}}$) the applied magnetic field, inducing an axial (ΔB_z) and an azimuthal (B_θ) magnetic field, respectively (Fig. 2a). The relative magnitudes of $j_{\theta\text{-net}}$ and $j_{z\text{-net}}$ will depend on the ratio of the azimuthal (v_θ) and axial (v_z) velocity components of the beam electrons. During the beam pulse, the plasma is heated by direct beam-plasma interactions[5] as well as ohmic dissipation of plasma currents[6] (Fig. 2b). As the beam current decreases, the dB/dt of the decaying beam induces a change in plasma current that opposes the change in beam current. The high conductivity of the heated plasma demands that these changes be almost equal, in order to conserve magnetic flux (Fig. 2c), thus maintaining the current configuration established during the beam pulse. For a sufficiently large $j_{\theta\text{-net}}$, ΔB_z is strong enough to produce reversal of the applied field on axis (i.e. $|\Delta B_z| \geq 1.0\ B_o$). If the chamber has conducting end walls, the field lines must close inside them, and the reversed-field geometry shown in Fig. 2d is formed. The magnitude of ΔB_z can be calculated from the net axial current, $I_{z\text{-net}}$, the azimuthal to axial beam velocity ratio, v_θ/v_z, and the layer radius, r_p^1;

$$\Delta B_z = \frac{\mu_o I_{z\text{-net}}}{2\pi r_p} \frac{v_\theta}{v_z} . \qquad (1)$$

The combination of the applied axial field, the induced axial field, and the induced azimuthal field, leads to an elongated cross-section toroidal plasma configuration. Such a field configuration is expected to exhibit favorable confinement properties for high θ plasmas.[7]

The condition for the sequence of events described above to occur is:

$$\tau_{D1} < \tau_{beam} < \tau_{D2}, \qquad (2)$$

where τ_{beam} is the beam duration, and τ_{D1} and τ_{D2} are the magnetic field decay times in the plasma before and after beam passage, respectively. For diffusive decay, τ_{Di} is related to the plasma conductivity, σ_i, and the characteristic length, x, by

$$\tau_{Di} = 4\mu_o \sigma_i x^2 .$$

It can be seen that for a typical relativistic electron beam of 50 nsec duration, injected into a system with a characteristic length of a few cm, the target gas must be initially neutral or only very weakly ionized to satisfy the first inequality in Eq. (2), whereas a plasma with final electron temperature exceeding 1 eV is sufficient to satisfy the second. Thus, the beam is not required to deposit much of its energy as heat, but rather to act as a vehicle to transport magnetic

energy into the system, which in turn remains there long after beam passage.

The induced plasma currents will decay on a time scale determined by the plasma conductivity. Therefore, in the absence of significant loss mechanisms, their dissipation will result in further plasma heating, and the configuration should persist for the characteristic magnetic diffusion time of the geometry. It can be seen, then, that in this system the induced magnetic field plays a dual role; 1) it provides the plasma confinement and 2) it acts as a store for the beam's energy, which can then be converted into plasma thermal energy through resistive dissipation. This latter effect was proposed and then observed in earlier rotating beam experiments by Kapetanakos, et al,[8] which achieved field reversed configurations having a duration of less than 1 μsec.

In the rotating beam experiment of Roberson, et al,[9] strong reversals of the applied field ($|\Delta B_z| > 4B_o$) with lifetimes of 2 μsec were observed. It was also found that $I_{z\text{-net}}\, v_\theta/v_z$, and consequently ΔB_z, was independent of the applied magnetic field.

To summarize the experimental results presented here, the formation of an annular plasma has been documented with end-on streak and framing photographs, and radial Thomson scattering scans. The formation of field reversing layers (defined as $|\Delta B_z| > 1.0B_o$) with a persistence time in excess of 5 μsec has been evidenced by local magnetic probes and several diamagnetic loops. Typical layer cross-section length-to-width ratios are equal to 40 cm/2.0 cm = 20. That this field configuration is induced by plasma currents, rather than trapped beam electrons, is indicated by the absence of hard x-ray emission after beam passage.

The external magnetic field measurements and diamagnetic loop data are fitted to an equilibrium model to estimate the radial profile of the fields and plasma pressure. End-on framing photograph measurements of the plasma radial dimensions, Thomson scattering measurements of $nkT_{e\perp}$ on axis and 2.5 cm off axis, and CO_2 laser interferometer determinations of $\int n.dl$, are found to be in agreement with this derived profile. After beam passage, ΔB_z remains relatively constant for 5 μsec until B_θ becomes small, at which point the annular plasma collapses radially. The measured 1/e decay time of 4 μsec, and concurrent two-fold increase in electron temperature (as determined by H_β line-to-continuum measurements, and verified at one instant by Thomson scattering) are consistent with classical processes. However, the axial confinement properties of this system cannot be inferred from the present experiment as the L/R time of the configuration is comparable to the time for plasma particles to be lost out the ends of the system. Since the ratio of L/R time to plasma end loss time increases at least as fast as T_e^2 (assuming classical processes), it is necessary to increase the electron temperature (for example, by an increase in beam current) to conclusively assess the long-term confinement properties of this system.

II. Experimental Apparatus

The experimental apparatus is shown in Fig. 3. A rotating relativistic electron beam is produced by injecting an annular beam from the TRITON accelerator[10] (1.2 MeV, 60 kA, 4 cm diameter, 60 nsec duration) through a non-adiabatic magnetic iron cusp[11] with a magnetic transition

half-width of 12 cm. The applied axial magnetic field, B_o, approaches uniformity at distances greater than 10 cm from each side of the cusp, and has a magnitude of 1.8 kG. The stainless-steel drift tube is 14.6 cm in diameter and terminated 80 cm from the cusp with a Faraday cup/calorimeter assembly. At the usual fill pressure of 85 mTorr H_2 (neutral atom density of 5.5×10^{15} cm^{-3}), net current generation was found to be maximized. Measurements with a miniature rotatable Faraday cup (similar in design to that described by Greenspan[12]) and observations with thin polyethylene damage rods (similar to those employed by Roberson[13]) show the beam has approximately equal azimuthal and axial velocity components and has a typical radius of 3.5 cm. These diagnostics, as well as damage on the main Faraday cup foil, also showed the axis of the beam-plasma system suffered shot-to-shot radial variations of as much as ± 2 cm. These variations are thought to be due to motion of the beam in the 15 cm long, 85 mTorr drift region between diode and cusp.

III. Experimental Results

End-on streak and framing photographs were taken through apertures mounted at the end of the drift tube opposite the diode. (In these experiments, the conducting end wall was defined by a transparent stainless steel grid, rather than the Faraday cup/calorimeter assembly.) As can be seen from Fig. 4, the plasma has an annular profile with radial dimensions comparable to those of the rotating beam (outer radius 3.5 cm, inner radius 2.0 cm) and is situated well away from the drift tube wall (radius 7.3 cm). Note, the plasma does not appear to undergo any gross radial motion as it decays; rather, the annular region appears

to fill in and then fade away. Streak photographs of extended duration show the plasma light lasts as long as 100 μsec, whereas the annular profile is maintained typically for 4 to 6 μsec. Supplementary side-on streak photographs (not shown) taken through a viewing port located 30 cm from the cusp also demonstrate the plasma to be annular and exhibit no gross radial motion.

Thomson scattering[14] measurements at 2.5 cm off axis and 400 nsec after beam injection show the plasma electrons to have, typically, densities of 5×10^{15} cm^{-3} and a Maxwellian velocity distribution corresponding to temperature of 5 eV. At these low temperatures, the plasma is expected to be located only in the light-emitting regions, and radial scans with Thomson scattering is consistent with the end-on photographs in Fig. 4. Because of the shot-to-shot variations of the electron beam and resulting plasma, detailed measurements of the radial profile could not be made. However, a series of 40 identical shots, 20 with the scattering system probing on the drift tube axis (r = 0), and 20 at 2.5 cm off axis show (errors indicate RMS scatter):

$$\overline{nkT_{e_\perp}} \quad (r = 0) = 7.2 \pm 5.2 \times 10^{15} \text{ eV/cm}^3, \tag{3a}$$

and

$$\overline{nkT_{e_\perp}} \quad (r = 2.5 \text{ cm}) = 17.1 \pm 15.0 \times 10^{15} \text{ eV/cm}^3. \tag{3b}$$

(The higher $\overline{nkT_{e_\perp}}$ at 2.5 cm off axis was manifested by an increase in

both electron temperature and density.) Data were taken between 400 and 800 nsec after beam injection. Note that the observation that the average $nkT_{e_\perp}$ on axis is greater than zero does not imply $nkT_{e_\perp}$ is greater than zero at the axis of the rotating beam: the shot-to-shot radial variations of the beam-plasma system and the finite radial extent (4 mm) of the scattering volume sometimes bri g the confinement region into the scattering volume, which is fixed in the drift tube frame. (In fact, 10% of the shots on axis show $nkT_{e_\perp}$ is less than 5×10^{14} eV/cm^3, that is essentially zero.)

Field reversal is inferred from the output of the diamagnetic loop (11.0 cm in diameter), which measures the change in axial magnetic flux, $\Delta\varphi$ (Fig. 5a). As the measured plasma pressure, $nkT_{e_\perp}$, can account for only 5% of the observed $\Delta\varphi$ (assuming $nkT_{e_\perp}$ as in Eq. 3b, and the annular radial profile depicted in Fig. 4b), the bulk of the diamagnetic signal is due to the induced axial magnetic field, ΔB_z. Employing a simple flux-conserving model,[15] in which the aximuthal plasma current layer has zero thickness, is located at a radius r_p, and is inside a flux conserving region of radius r_w, the voltage induced on an N-turn loop of radius r_L (such that $r_w > r_L > r_p$) terminated with passive integrator network of time constant RC, is (MKS units):

$$V = \frac{N\pi\,\Delta B_z}{RC}\,\frac{r_w^2(1-r_L^2/r_w^2)}{(r_w^2/r_p^2-1)}. \qquad (4)$$

Using Eq. 4, the diamagnetic signal depicted in Fig. 5a is sufficient to account for full cancellation of the applied field on axis ($\Delta B_z = -1.0\ B_o$)

for approximately 6 μsec (assuming r_p = 3.5 cm as indicated by the end-on photographs). At peak diamagnetic signal, ΔB_z = -3.3 kG or approximately -1.8 B_o. The loss of field reversal is concurrent with the observed collapse of the annular plasma in Fig. 4b.

The persistence time of the axial plasma current, as indicated by the output from a B_θ probe located 6.3 cm off axis, is shown in Fig. 5b. A characteristic feature of these experiments is that no appreciable decay of ΔB_z is seen until B_θ goes to zero. This result is discussed in Section V. These measurements show that $I_{z\text{-net}}$ = 45 kA, implying the plasma currents induced by the entrance of the beam are small compared to the beam current.

The observed induced change in axial magnetic field is consistent with other measurements. Using Eq. 1, with v_z/v_θ = 1 (determined from damage rod and miniature Faraday cup studies), $I_{z\text{-net}}$ = 45 kA, and r_p = 3.5 cm, the induced change is calculated to be ΔB_z = -2.9 kG or approximately -1.6 B_o.

To satisfy the skeptics, existence of field reversal was verified directly by measurements with a miniature (.3 cm diameter) local axial magnetic probe. The probe was insulated in a quartz tube, positioned on drift tube axis at the same axial position as the diamagnetic loop, and cantilevered from a rigid end plate located 1 meter downstream. It is generally desirable to obtain measurements of ΔB_z with such an on-axis probe, as opposed to a diamagnetic loop, since the former yields ΔB_z directly, whereas the latter only if a plasma radius is known. The probe output agrees well with the diamagnetic loop, however, as seen in Fig. 6, lower field reversals (ΔB_z approximately equal to -1.3B_o) and

faster decay times (approximately 2 μsec) were observed when this probe was installed. This effect is attributable to the shot-to-shot radial variations, which would allow this probe to intercept a portion of the rotating beam and plasma currents. (There is evidence in the reversed field theta pinch experiment of Linford[16] that an axial probe does not have to physically intercept the rotating currents in order to have a perturbing effect.) For this reason the on-axis probe was not installed during most of this investigation. A local axial magnetic probe was also positioned at 6.3 cm radius (1 cm inside the drift tube wall) to determine ΔB_z outside the field reversing layer. Such a probe did not perturb the plasma and indicated ΔB_z = + 300 G or approximately + .17 B_o, consistent with flux conservation inside the drift tube.

Three concentric diamagnetic loops with identical axial positions and RC networks were employed to determine the flux excluding area of the current layer. If this area is totally enclosed by the smallest of these diamagnetic loops, then by Eq. 4, the signal voltages from all three loops are proportional to $(1 - r_L^2/r_w^2)$. In Table 1, normalized outputs of the three diamagnetic loops are compared with the calculated values. Agreement between calculation and experiment for these several shots indicates the flux excluding area is always inside the innermost loop (radius 5.9 cm). Allowing for the maximum radial variation of ± 2 cm, these results suggest the layer radius cannot exceed 3.9 cm, in keeping with the previously estimated value of 3.5 cm.

That these field reversing layers are induced primarily by plasma currents rather than trapped relativistic beam electrons can be ascertained from hard x-ray studies. The emission from a 1 mm diameter tungsten

wire placed across the drift tube at a position 30 cm from the cusp is shown in Fig. 7. Appropriate filters were used to discriminate against x-rays with energies less than 70 keV. The presence of the tungsten target does not affect either the layer lifetime or strength. As the target absorbs all of the beam electrons within 1 μsec, this result suggests trapped beam electrons play a minor role in layer persistence. Furthermore, comparison with Figs. 5a and 5b shows the emission exhibits neither the lifetime nor the temporal dependence of either the azimuthal or axial currents.

CO_2 laser interferograms[17], used to determine the plasma line density along a major diameter at an axial position of 30 cm, are shown on two different time scales in Fig. 8. Due to limitations of the detector response, the initial rise of the plasma on the beam time scale cannot be seen. After a comparatively featureless period of 10 μsec, during which the onset of "partial fringes" is observed, the interferometer exhibits a normal decay, as manifested by several full amplitude fringes. It was ascertained that the quiescent phase corresponds to a period when the plasma refracts the CO_2 laser beam out of the diagnostic arm path. (The mechanism for this refraction is not well understood.) In keeping with the end-on photography (Fig. 4) the partial fringes may correspond to radial contraction, but not gross radial motion (i.e., variation in radial position) of the plasma. Assuming, then, that only the full amplitude fringes correspond to a decay in density, the resulting plasma line density, averaged over 20 shots, is inferred to be:

$$\int n.d\ell = 66 \pm 13 \times 10^{15} \text{ electrons/cm}^2.$$

Note from Fig. 8b plasma is present for some 100 μsec after beam injection,

a result consistent with extended end-on streak photographs.

IV. Comparison with Equilibrium Model

A toroidal equilibrium model has been employed to determine the equilibrium configuration consistent with the experimental data. Input to the model include the flux change measured by the diamagnetic loop, and the measured ΔB_z and B_θ fields determined by local magnetic probes placed just inside the drift tube wall. The model output is found to be in agreement with the experimentally determined plasma radial energy density profile.

In this model, the plasma pressure is assumed to be balanced by the Lorentz force at all points:

$$\vec{j} \times \vec{B} = \vec{\nabla} P. \tag{5}$$

A cylindrical (r,θ,z) coordinate system with $\vec{e}_\theta$ the unit vector in the toroidal (azimuthal) direction (see Fig. 9) is chosen. The plasma boundary, where the plasma pressure is zero, is assumed to be a rectangle, whose center is located at $r = r_p$ and $z = 0$. The cross-section dimensions are such that $-b \leq z \leq b$ and $r_p - a \leq r < r_p + a$.

Consistent with the assumption of axisymmetry ($\partial/\partial\theta = 0$), the magnetic field is expressed in terms of the poloidal (axial) flux function $\psi(r,z)$:

$$B = \frac{I(\psi)}{r} \vec{e}_\theta + \frac{1}{r} \vec{e}_r \times \vec{\nabla} \psi, \tag{6}$$

where $I(\psi)$ is a function of the poloidal flux. With the field expressed in this form and the use of Maxwell's equations, force balance (Eq. 5) can be written as a partial differential equation for $\psi(r,z)$[18],

$$r \frac{\partial}{\partial r} \frac{1}{r} \frac{\partial \psi}{\partial r} + \frac{\partial^2 \psi}{\partial z^2} = - 4\pi r^2 \frac{\partial P}{\partial \psi} - I \frac{\partial I}{\partial \psi} . \tag{7}$$

To proceed further, it is necessary to know $P = P(\psi)$ and $I = I(\psi)$. Following Maschke[19], a quadratic dependence for P and I is assumed with normalization such that

$$\begin{aligned} P &= P_1 \psi^2 , \\ I^2 &= I_o^2 + M\psi^2 , \end{aligned} \tag{8}$$

where P_1, I_o and M are constants. In addition, the variation in the z direction is assumed to be harmonic, i.e.:

$$\psi(r,z) = \psi(r) \cos(kz). \tag{9}$$

The boundary condition that $P = 0$ at $z = \pm b$ implies that $kb = (2m + 1)(\pi/2)$. In this calculation m is taken to be zero and, to be consistent with axial diamagnetic loop data to be presented in Section V, $b = \ell/2 = 20$ cm. Eq. (7) can be put in a more convenient form by changing the radial variable to $\rho = \sqrt{2\pi P_1 r^2}$. Using Eqs. (8) and (9),

it is found that:

$$\frac{d^2\psi}{d\rho^2} + \left(\left(\frac{2\eta}{\rho} \right) - 1 \right) \psi = 0. \qquad (10)$$

Here η is a characteristic eigenvalue, where:

$$\eta = \frac{k^2 - M}{4(\pi P_1)^{\frac{1}{2}}} . \qquad (11)$$

Although this equation has analytic solutions[13], it is more convenient to solve it by numerical integration. Integration is carried out using the experimentally determined values of ΔB_z and B_θ at 6.3 cm off axis and the change in flux inside r = 5.5 cm (i.e., the diamagnetic loop signal) to infer the radial position (at z = 0) of the outermost closed flux surface, $\psi(R_o + a, 0) = 0$. Eq. (10) is then integrated radially inward to $r = R_o - a$.

In Figure 10, the calculated curves of the radial variation of $nkT_{e\perp}$ (defined as 0.5 P) and B_z are shown as the solid and broken curves, respectively. Best fit to the observed magnetic field data is found for R_o = 2.5 cm, a = 1.75 cm and $\eta = 0$.

As summarized in Table 2, the predictions of this model are found to be in agreement with the experimental observations at t = 400 to 800 nsec. (The plasma characteristics were constant over this time.) The expected average values for $nkT_{e\perp}$ at a fixed radial position are estimated from the predicted electron energy density radial profile (solid curve, Fig. 10), and a C&P random number generator (to simulate

the shot-to-shot radial variations). Based on damage pattern and streak photographs, it is assumed that the plasma is formed away from the axis with displacement δr, the average of which is $\langle \delta r \rangle = 1.0$ cm and the maximum of which is $|\delta r|_{max} = 2.0$ cm. Using 20 random numbers for δr, normalized such that $\langle \delta r \rangle = 1$, the expected pressure at $r = \langle r \rangle + \delta r$ is calculated for $\langle r \rangle = 0$ and $\langle r \rangle = 2.5$ cm. These results are in agreement with the measured values, as are the predictions of the minimum and maximum energy densities. Furthermore, the line density, $\int n.dl$, (derived assuming n_e and $T_{e\perp}$ have the same radial dependence) is consistent with CO_2 laser interferometry data.

The magnetic field profile (broken curve in Fig. 10) predicts $\Delta B_z = -3.9$ kG, or $-2.17\ B_o$, a somewhat stronger reversal than that calculated from the simple flux conservation model in Eq. 4. The discrepancy is due to the assumption of an infintesimally thin current layer in the flux conservation model and the value from the equilibrium model is more reliable.

The reversed field configuration does not exhibit any gross unstable motions. However, after formation, the configuration undergoes small amplitude ($\pm$ 10%) radial oscillations, as manifested on the diamagnetic loop output. The oscillation period is consistent with that predicted by the theory of Chu, et al.[20], in which it was shown that a rotating beam can excite the magnetosonic mode of the plasma. The period of this mode is predicted to be:

$$\tau_m = (2a/V_m)\left[1 + (\pi c)^2/(\ell\omega_{pi})^2\right]^{-\frac{1}{2}}, \qquad (12)$$

where ω_{pi} is the ion plasma frequency, $V_m = V_A(1 + \beta)^{\frac{1}{2}}$ (V_A is the Alfven velocity, $\beta = 2\mu_o nkT_\perp/B_o^2$), and ℓ and r are respectively the length and radius of the beam. With the parameters of this experiment, $\beta = .5$, $n_i = 5 \times 10^{15}$ cm^{-3}, $a = 3.5$ cm, $\ell = 40$ cm, and $B_o = 1.2$ kG (at the plasma/vacuum interface, see Fig. 10), it is found that $\tau_m = 1.6$ μsec, in good agreement with the observed period of approximately 2 μsec. Calculations indicate the radial extent of these oscillations is on the order or ± .5 cm. Of importance here is that these oscillations do not grow in time, suggesting that the system has "found" a stable equilibrium.

The experimental observations, then, confirm that an equilibrium elongated cross-section toroidal configuration has been produced. The resulting toroidal cross-section is non-circular with a length-to-width ratio, b/a, approximately equal to 20. The $z = 0$ (midplane) cross-section experimental average value of $\beta \equiv < 2\mu_o nk(T_e + T_i)_\perp/B_o^2 >$ is approximately .5. Unlike a Tokamak-type configuration, the poloidal (axial) field on the outer closed flux surface is larger than the toroidal (azimuthal) field. Nevertheless, the small aspect ratio (r_p/a on the order of 1.5) and large length-to-width ratio yield an effective value for q of 4 on the outer flux surface, where

$$q \equiv 4(b + a)\, B_\theta/2\pi r_p B_z . \qquad (13)$$

Thus, one would expect this configuration to be magnetohydrodynamically stable.

V. The Decay of the Configuration

After the beam has left, the induced magnetic configuration decays as a result of the resistive dissipation of the plasma currents. The signals from the diamagnetic loop (which measures B_z external to the loop) and the B_θ probe (Fig. 5) do not decay exponentially because the changing magnetic fields cause a change in the plasma equilibrium. The decay of j_z decreases B_θ^2, changing the force balance to move the plasma outward, whereas the decay of j_θ will cause B_z^2 on axis to decrease faster than B_z^2 outside the layer, and thus move the plasma inward. Thus it is reasonable to expect a net outward motion of the plasma which compresses the (decaying) axial return flux against the wall, keeping B_z outside the loop approximately constant until B_θ has become small, at which point the plasma column contracts. This explanation is consistent with the framing photographs (Fig. 4b), which show an increase in the mean plasma radius in the first 4 μsec and subsequent contraction; and a simple pressure balance model, which correctly predicts the temporal behavior of the diamagnetic loop signal shown in Fig. 5a.

The observed late time 1/e decay times for both B_θ and ΔB_z of approximately 4 μsec are consistent with classical resistive decay of the currents, assuming the electron temperature of 5 eV measured by Thomson scattering. However, at these low temperatures, the L/R time of the configuration τ_D, is also comparable to τ_s, the time for plasma to free stream out of the ends of the apparatus (given by $\ell/2c_s$ where ℓ is the length and c_s the sound speed), assuming no axial confinement. Hence, although it is believed the field lines are closed

at the ends, this set of experiments does not provide direct evidence of plasma containment. Since

$$\tau_D/\tau_s \propto T_e^{3/2}/T_e^{-1/2} = T_e^2, \tag{14}$$

to verify axial containment in the present experiment requires T_e to exceed 30 eV.

As is to be expected, the dissipation of magnetic energy leads to an increase in plasma temperature, as indicated by the data in Fig. 11, which shows the results of H_β line-to-continuum measurements. Light was collected along a chord 2.5 cm off the drift tube axis, and wavelength resolved with three 27 Å wide channels, one at the H_β line (4861 Å) and the other two at 4861 ± 27 Å. As seen in Fig. 11, the electron temperatures indicated by this diagnostic are in agreement with those predicted by Thomson scattering. The most salient feature, however, is the 80% increase in T_e over the layer lifetime. The amount of electron heating that can take place through the induced current decay can be calculated assuming classical resistivity. Using the measured initial electron temperature of 5 eV at full ionization, calculations of the total energy deposited into the plasma, i.e., $j_z^2 \eta \tau V$, where j_z is the axial current, η the classical resistivity, τ the appropriate time, and V the appropriate volume, yield a $\Delta E/\text{pair} \equiv T_e + T_i$ of approximately 12 eV. Assuming a classical electron-ion relaxation time ($T_e = T_i$ on these time scales) yields a final electron temperature of approximately 11 eV, consistent with that observed in Fig. 11.

It is not surprising that the resistivity observed in these experiments

is classical, as at these low temperatures, single particle Coulomb collisions dominate. For the classical collision frequency to be less than the lower hybrid frequency, for example, the electron temperature must exceed 55 eV. (The lower hybrid mode[21] is the most applicable instability for this geometry as it yields an anomalous cross-field resistivity and can readily be excited whenever the drift velocity exceeds the ion thermal velocity.)

The layer length appears to decrease as the system decays. The outputs of three diamagnetic loops placed at various axial positions are shown as a function of time in Fig. 12. At 500 nsec after beam injection, the layer strength 40 cm from the cusp is approximately 30% of that at 10 cm from the cusp, suggesting a characteristic length of 40 cm. The signals from the loops at the ends of the layer decrease faster than those from the one near the center. This observation can be explained by modeling the azimuthal currents as a coil which tends to maximize its self inductance, i.e. contract axially. This tendency is balanced by the pressure of the confined plasma, which maintains the elongated geometry. (This may explain why the field reversing layers in this experiment do not coalesce into a "bicycle tire" geometry characteristic of field reversing relativistic electron rings[22], which do not contain a warm plasma.) Therefore, as plasma pressure is lost, the layer length should decrease, as observed.

VI. Energy Accounting

An attempt was made to ascertain the partitioning of the rotating beam energy after passage through its self-made plasma. The energy

accounting is not yet complete, as can be seen in Table 3. These numbers were calculated at 400 nsec, when the system is thought to be in quasi-steady state. A layer of inner and outer radii 2.0 and 4.0 cm, respectively, and axial length 40 cm was used in these calculations. Of the original 1420J in the beam, 40% is lost in passing through the cusp. This low transfer efficiency is thought to be due to the broad cusp transition width and long drift region between diode and cusp. Of the 845J injected, 20% is deposited in the plasma and induced fields, 42% passes straight through the system and 38% is unaccounted for. One of the most important tasks of future experiments is to account for the "lost" energy and to improve the fraction of beam energy that is deposited in the plasma. However, using the energy accounting of Table 3, some information may be inferred about the rotating beam-plasma energy transfer during the beam pulse:

1. With a cathode radius of 2 cm and an observed damage radius on polyethylene rods of 3.5 cm, radial expansion producing large amplitude Alfven wave heating[23] is a possible energy transfer mechanism. This in turn implies the ions can have a substantial temperature. This aspect will be investigated further in a future experiment.

2. High electron temperatures are observed on a time scale less than four times the beam pulse duration, indicating a rapid beam-to-plasma energy transfer. Classical processes, such as Coulomb scattering of beam primary electrons or classical resistive dissipation of induced plasma return currents, cannot account for such a rapid energy transfer. In the latter case, computations of ionization and heating by return current dissipation have been performed using a code described else-

where.[24] It is found that such rapid ionization and heating in the presence of classical resistivity alone would require plasma current densities in excess of 15 kA/cm^2, an order of magnitude larger than can reasonably be expected in this experiment. On the other hand, turbulent resistivities, obtained from models of the e-e, ion acoustic, or lower hybrid drift modes, are capable, either individually or in combination, of producing the observed ionization levels and electron temperatures with current densities of only 2 kA/cm.^{2} This current density is more in keeping with those inferred from the present experiment (0.8 - 1.6 kA/cm^2).

3. It should be noted again that the beam deposits most of its energy into the induced magnetic field (103 J of magnetic energy vs 24 J of plasma energy) and that dissipation of the induced currents is a significant heating mechanism in this experiment.

VII. Acknowledgments

The authors wish to acknowledge helpful discussions with Dr. K. R. Chu, Dr. Carl Ekdahl, Dr. J. R. Greig, Dr. William Grossman, Dr. Rulon Linford, Dr. Charles Roberson, Dr. Scott Robertson and Dr. Norman Rostoker, and wish to acknowledge the technical assistance of Mr. R. M. Jones and Mr. A. K. Kinkead.

VIII. References

1. D. A. Hammer, A. E. Robson, K. A. Gerber and J. D. Sethian, Phys. Lett. 60A, 31 (1977).
2. G. Becker, A. Eberhagen, O. Gruber, K. Herold, J. M. Peiry, H. Rohr,

R. Wilhelm and H. Zwicker, in Plasma Physics and Controlled Nuclear Fusion Research, (International Atomic Energy Agency, Vienna, 1975) Vol. III, p. 47.

3. D. L. Book et al. Plasma Physics and Controlled Nuclear Fusion Research 1976 (6th Conf. Proceedings, Berchtesgaden, 6-13 Oct. 1976) IAEA Vienna 1977 Paper E-19-1.

4. F. H. Coensgen, J. F. Clauser, D. L. Correll, W. F. Cummins, C. Gormezano, B. G. Logan, A. W. Molvik, W. E. Nexsen, T. C. Simonen, B. W. Stallard, and W. C. Turner, in Plasma Physics and Controlled Nuclear Fusion Research. (International Atomic Energy Agency, Vienna, 1977) Vol. III, p. 135.

5. L. E. Thode, Phys. Fluids 19, 831 (1976), and K. Papadopoulos, Phys. Fluids 18, 1769 (1976).

6. R. V. E. Lovelace and R. N. Sudan, Phys. Rev. Lett 27, 1256 (1971).

7. H. P. Furth, Nucl. Fusion 15, 487 (1975).

8. C. A. Kapetanakos, W. M. Black, and C. D. Striffler, Applied Physics Letters 26, 368 (1975).

9. C. W. Roberson, D. Tzach, and N. Rostoker, U.C.I. Technical Report No. 77-48, University of California, Irvine, California 90345.

10. J. K. Burton, J. J. Condon, M. D. Jevnager, W. H. Lupton, and T. J. O'Connell, in Proceedings of the Symposium on Engineering Problems of Fusion Research, (IEEE, New York, 1974) p. 613.

11. G. Schmidt, Phys. Fluids 5, 994 (1962); and R. E. Kribel, K. Shinsky, D. A. Phelps and H. H. Fleischmann, Plasma Physics 16, 113 (1974).

12. M. A. Greenspan, Ph.D. thesis Cornell University, Ithaca, N.Y. (1976).

13. C. W. Roberson, G. Saenz, and D. Tzach, UCI Technical Report 76-41, University of California, Irvine, California 90345.

14. K. A. Gerber, Naval Research Laboratory Memorandum Report No. 2818, Washington, D. C. (1974).

15. K. A. Gerber, J. D. Sethian, and D. N. Spector, Rev. Sci. Inst., to be published.

16. R. K. Linford, D. A. Platts, E. G. Sherwood, in Proceedings of the IEEE International Conference on Plasma Science, (IEEE, New York, 1977), p. 124.

17. D. N. Spector, Naval Research Laboratory Memorandum Report No. 3214, Washington, D. C. (1975).

18. H. Grad and H. Rubein, in Proceedings of the Second United Nations International Conference on the Peaceful Uses of Atomic Energy, (United Nations, Geneva, 1958), p. 190.

19. E. K. Maschke, Plasma Physics 15, 535 (1973).

20. K. R. Chu, C. A. Kapetanakos, and R. W. Clark, App. Phys. Lett. 27, 185 (1975).

21. R. C. Davidson and N. T. Gladd, Phys. Fluids 18, 1327 (1975).

22. H. A. Davis, R. A. Meger and H. H. Fleischmann, Phys. Rev. Lett. 37, 542 (1976).

23. K. R. Chu and N. Rostoker, Phys. Fluids 17, 813 (1974).

24. D. A. Hammer, A. E. Robson and A. W. Ali, private communication.

Table I

Comparison of calculated and observed diamagnetic signal for the radially resolving diamagnetic loops. Observed signals are taken from four shots, at varying times after electron beam injection. All data are normalized to the signal from the r_L = 7.14 cm loop. Conducting wall radius is 7.3 cm.

Diamagnetic Loop Radius (cm)	Calculated Diamagnetic Signal	Observed Diamagnetic Signals			
7.14	1.0	1.0	1.0	1.0	1.0
6.67	4.0	3.7	3.7	3.8	4.2
5.93	7.8	7.6	7.6	7.8	7.6

Table II

Summary of comparison between experimentally determined and theoretically predicted quantities, based on an equilibrium model consistent with observed magnetic field data. Data taken between 400 to 800 nsec after beam injection.

Quantity	Method of Determination	Experimental Observations	Theory
Radial Dimensions	End-on Framing Photographs	r_1 = 2 cm r_2 = 3.5 cm	r_1 = 1.5 cm r_2 = 4 cm
Position of j_θ Maximum	Damage Rods, Concentric Loops	r_p = 3.5 cm	r_p = 3.25 cm
$\overline{nkT_{e\perp}}$ (r = 0)	Thomson Scattering	$7.2\pm5.2\times10^{15}$ eV/cm^3 [a]	$6.5\pm1.7\times10^{15}$ eV/cm^3 [d]
$\overline{nkT_{e\perp}}$ (r=2.5 cm)	" "	$17.1\pm15.0\times10^{15}$ eV/cm^3 [a]	$23\pm1.4\times10^{15}$ eV/cm^3 [d]
$nkT_{e\perp min}$ (r=0)	" "	$<5\times10^{14}$ eV/cm^3 [b]	0
$nkT_{e\perp max}$ (r=2.5 cm)	" "	60×10^{15} eV/cm^3 [c]	55×10^{15} eV/cm^3
$\int n.dl$	CO_2 Interferometer	$66\pm13\times10^{15}$ elec/cm^2	60×10^{15} elec/cm^2
ΔB_z on axis	Diamagnetic Loop	-1.8 kG	-2.1 kG

a Average of 20 shots

b Average of three lowest

c Average of three highest

d 20 "random" shots

Table III

Energy Accounting

Form of Energy	Method of Determination	Total Energy
Diode Energy	Diode Voltage and Current Monitors; Calorimeter	1420 J.
Energy Lost Through Cusp	Calorimeter	580 J.
Total Rotating Beam Energy Injected		840 J.
Magnetic Field; ΔB_z	Diamagnetic Loops	45 J.
Magnetic Field; B_ϑ	B_ϑ Probes	60 J.
Plasma Particles	Thomson Scattering (Assumes $T_{e\perp}=T_{i\perp}$ = 5eV)	25 J.
Plasma Ionization Energy	Numerical Computation, 25 eV per e-i pair	45 J.
Total Energy into Particles and Fields		175 J.
Beam Energy After Passage Through Drift Region	Calorimeter	360 J.
Total Energy Unaccounted For		305 J.

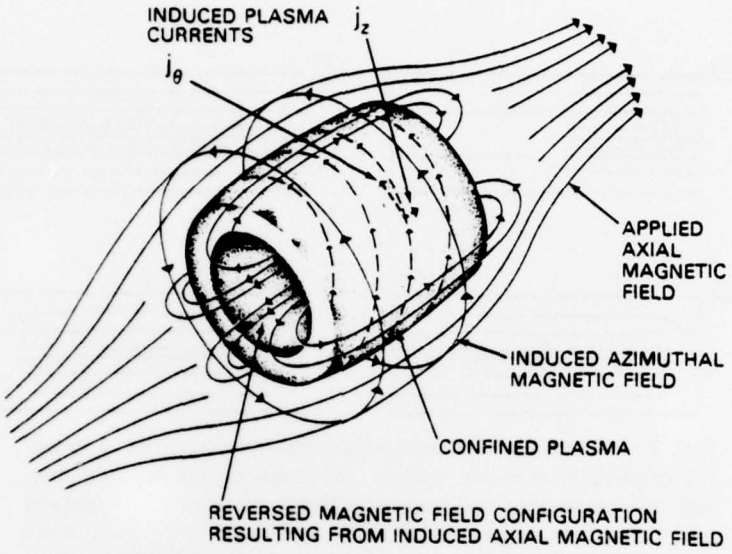

Fig. 1 — Rotating relativistic electron beam induced axial ($j_{z\text{-net}}$) and azimuthal ($j_{\theta\text{-net}}$) plasma currents and the resultant azimuthal (toroidal) field, B_θ, and axial (poloidal) field B_z, respectively

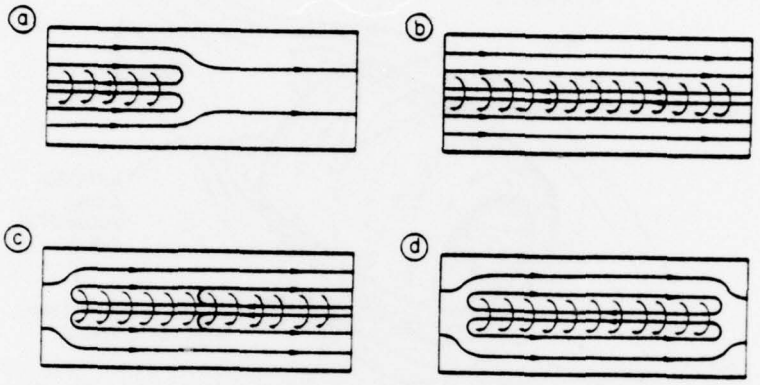

Fig. 2 — Creation of reversed-field configuration by a rotating relativistic electron beam: (a) beam enters initially neutral gas producing self-magnetic fields; (b) plasma is formed and heated; (c) beam leaves the system, inducing plasma currents which persist in the high conductivity plasma, resulting in further plasma heating as they decay. (For simplicity, the induced J_z and resultant B_θ outside the confined plasma have not been shown.)

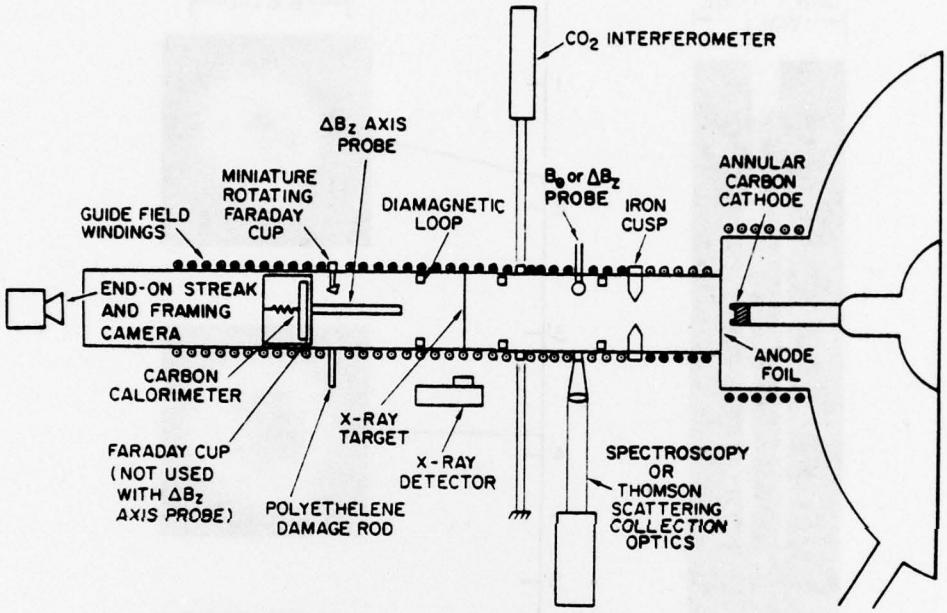

Fig. 3 — The experimental facility

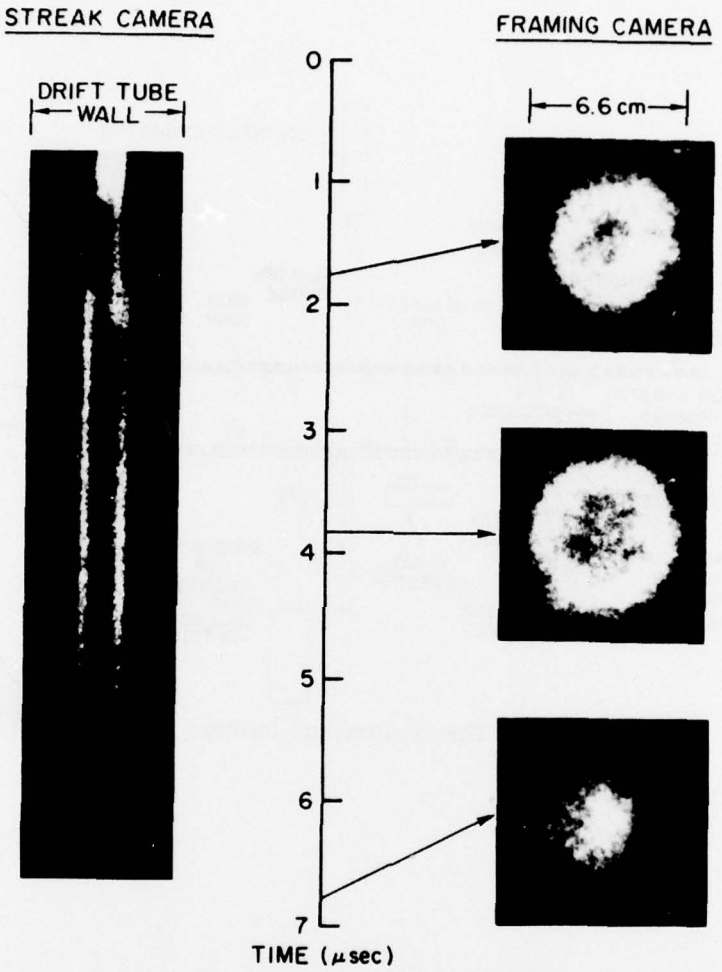

Fig. 4 — End-on streak (a) and framing (b) photos of plasma column

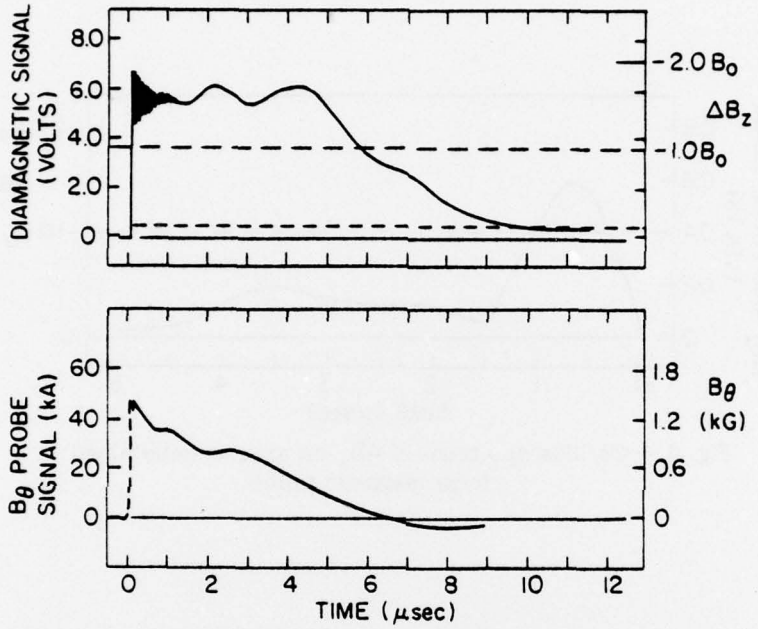

Fig. 5 — Typical oscilloscope traces showing magnitude and temporal behavior of the induced (a) axial and (b) azimuthal fields. Trace (a) is the diamagnetic loop signal. The lower dashed line indicates the diamagnetism accounted for by the electron energy density as determined from Thomson scattering. The remainder of the diamagnetic signal is due to rotating beam-induced field reversing plasma current layers. The right hand vertical scale gives the change in axial field on axis, assuming a layer radius of 3.5 cm, in terms of the applied field, B_o. Trace (b) is calibrated both in units of the azimuthal field (kG) and the axial current (kA).

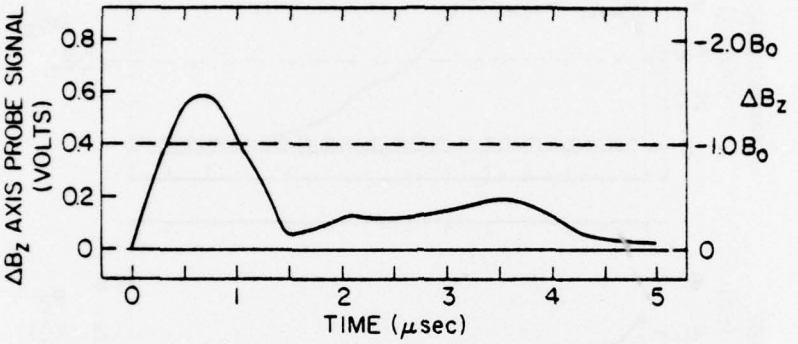

Fig. 6 — Oscilloscope trace of ΔB_z on axis, as determined by a local magnetic probe

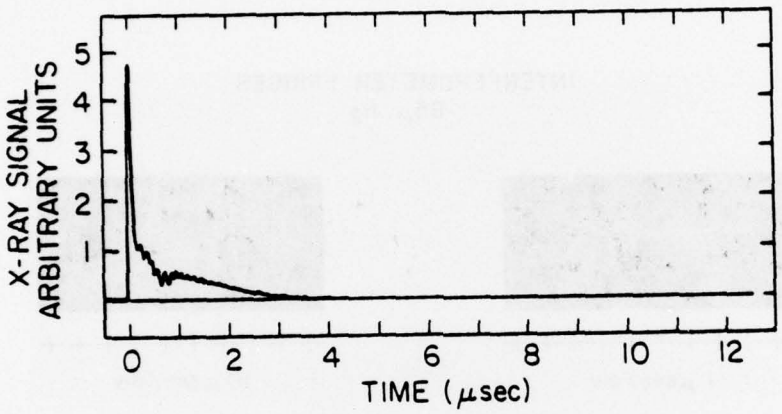

Fig. 7 — Temporal dependence of hard x-ray emission from a 1 mm diameter tungsten wire placed across the drift tube

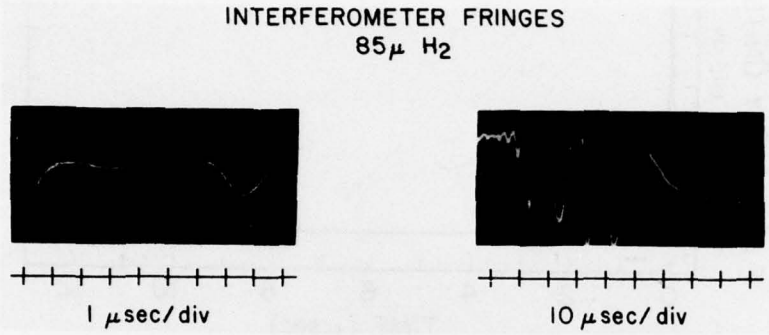

Fig. 8 — CO_2 laser interferometer traces on 1 μsec/div (left) and 10 μsec/div (right)

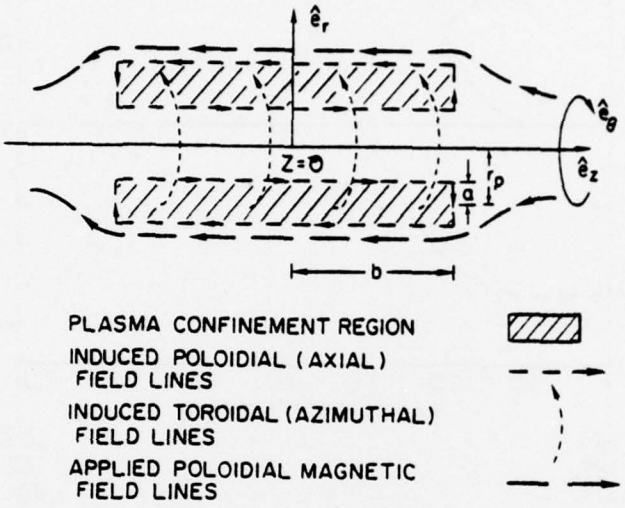

Fig. 9 — Geometry used in equilibrium model

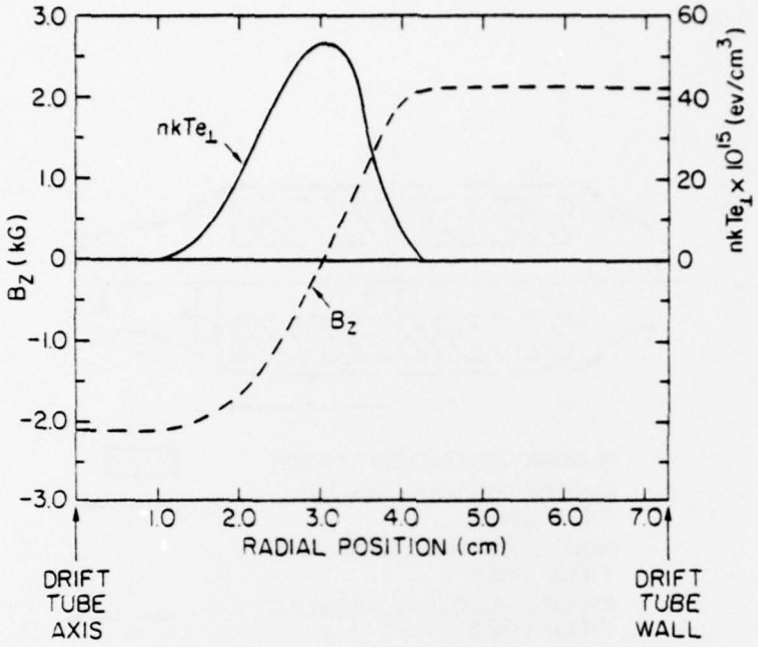

Fig. 10 — Electron energy density profile (solid curve) and axial magnetic field profile (broken curve) predicted by an equilibrium model fitted to the magnetic field measurements.

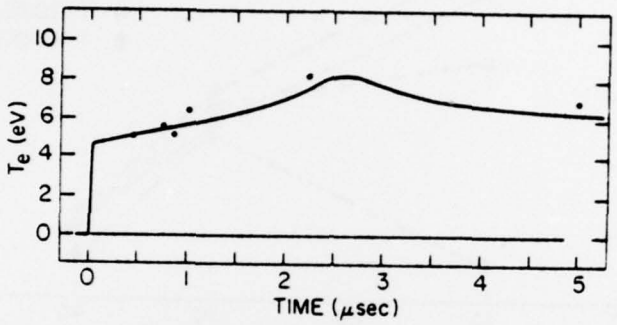

Fig. 11 — History of the electron temperature after beam injection. T_e is obtained from H_β line-to-continuum studies. The points show Thomson scattering data, each data point being the average of three shots.

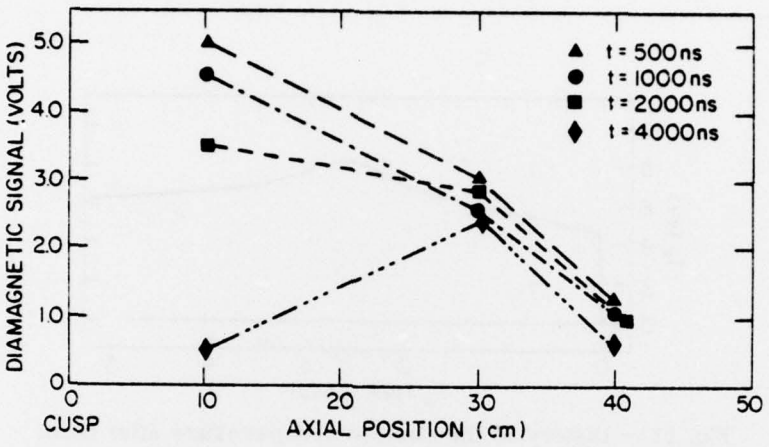

Fig. 12 — Diamagnetic signal as a function of axial position and time after beam injection